Rapid Communications

Charge confinement and thermal transport processes in modulation-doped epitaxial crystals lacking lattice interfaces

Elizabeth Radue,[1] Evan L. Runnerstrom,[2,3] Kyle P. Kelley,[2,3] Christina M. Rost,[1] Brian F. Donovan,[4] Everett D. Grimley,[2] James M. LeBeau,[2] Jon-Paul Maria,[2,3] and Patrick E. Hopkins[1,5,6,*]

[1]*Department of Mechanical and Aerospace Engineering, University of Virginia, Charlottesville, Virginia 22904, USA*
[2]*Department of Materials Science, North Carolina State University, Raleigh, North Carolina 27695, USA*
[3]*Department of Materials Science and Engineering, Pennsylvania State University, State College, Pennsylvania 16801, USA*
[4]*Department of Physics, United States Naval Academy, Annapolis, Maryland 21402, USA*
[5]*Department of Materials Science and Engineering, University of Virginia, Charlottesville, Virginia 22904, USA*
[6]*Department of Physics, University of Virginia, Charlottesville, Virginia 22904, USA*

(Received 27 December 2018; published 29 March 2019)

Heterogeneous nanosystems offer a robust potential for manipulating various functional material properties, beyond those possible from their individual constituent materials. We demonstrate the formation of a class of materials with a homogeneous lattice but spatially heterogeneous electrical functionality; specifically, we develop epitaxial modulation-doped thin films in which the spatial separation of electronic charge densities is achieved without perturbing the parent crystal's compositional or structural homogeneity. Unlike the previous realizations of modulation doping in crystals, our materials demonstrate periodic layering of spatially segregated, varying electronically donor-doped regions in a single compositionally and structurally homogenous single-crystalline lattice. We demonstrate the formation of "modulation-doped epitaxial crystals" (MoDECs) using alternating layers of doped cadmium oxide, and the ability to spatially confine regions of variable carrier concentration via low potential-energy barriers in a spatially homogeneous, epitaxial crystal with a chemically and structurally homogenous lattice (i.e., no chemical or structural lattice interfaces). The low potential energy that confines electrons within the doped layers coupled with the crystalline nature of the MoDECs and lack of lattice interfaces presents a platform to study the electron thermal boundary resistances at low-energy electronic barriers. We find that the electron interfacial density does not impede thermal conductivity, despite evidence that the doped layers retain their carrier concentrations. Thus, the negligible thermal boundary resistances at the electronic interfaces result in the thermal conductivities of the MoDECs being related to only a series resistance sum of the thermal resistances of each of the individual layers, with no thermal resistances from the electronic boundaries that maintain charge separation. This is in stark contrast with other nanoscale multilayer materials, where thermal boundary resistances at the internal material interfaces reduce the thermal conductivity of the multilayer compared to that of the parent materials. The ability to modulation dope epitaxially grown films with no structural heterogeneity in the lattice will further enable unique platforms for mid-IR photonics, such as hyperbolic metamaterials, optical filters with spatially discrete optical absorption, or energy harvesting based on charge injection across modulation-doped interfaces.

DOI: 10.1103/PhysRevMaterials.3.032201

Superlattices and other periodic material multilayers are arguably some of the most studied nanostructures in terms of their functional properties. This unique class of nanomaterials has attracted considerable attention over the past few decades since they provide the ability to manipulate material properties at the length scales of the fundamental carriers of energies. For example, the periodic patterning of alternating nonmetals and/or metals, with periodicities on the order of nanometers to micrometers, has led to impeccable control over photon, electron, and/or phonon transport that has resulted in promising solutions for thermoelectric devices [1,2], quantum cascade and vertical cavity surface emitting laser diodes [3–6], amplified photodetectors [7–11], and radiation resistant coatings [12,13].

Along these lines, the electronic and thermal transport properties of superlattices have been of fundamental interest to study unique properties of electrons and phonons. For example, researchers have used metal-metal superlattices to validate the Wiedemann-Franz law at interfaces [14], and demonstrate the exceptionally large electron-electron thermal boundary conductance across metal/metal interfaces [12,13]. In nonmetal/nonmetal superlattices, a wealth of studies have demonstrated the strong reduction in thermal conductivity that can occur due to phonon-boundary scattering [15–20], while more recent works have experimentally demonstrated a combination of ballistic and coherent phononic transport that can occur in these periodic structures [5,20], along with the existence of a minimum in the thermal conductivity as a function of period thickness [21]. These unique phonon processes, the observation of which is enabled by the nanoscale design of the superlattices, provide evidence of miniband formation and shed insight into the wave-particle duality of phonons [22].

*Corresponding author: phopkins@virginia.edu

A more multifunctional form of compositionally layered semiconductor systems requires judicious doping of the semiconductor layers in constructing tailored photonic interactions or electronic transport. In particular, modulation doping of individual material layers in these superlattices, which leads to spatial separation of free carriers [23,24], has demonstrated the potential for improved functionality, such as an increased thermoelectric response using modulation-doped superlattices [25]. Moving beyond compositionally heterogeneous layered structures, modulation doping has been realized in three-dimensional (3D) solid solutions by varying cation compositions, e.g., $(Bi_xSn_{1-x}Se)_{1+d}TiSe_2$ [26], or by creating two-phase composites with doped and undoped nanoregions, e.g., BiCuSeO and $Bi_{0.75}Ba_{0.25}CuSeO$ or SiGe and Si [27–29]. In the former of these cases, the anisotropy, orientation, and natural layering of the crystalline unit cell enabled modulation doping, where in the latter case lattice interfaces between the two phases in the three-dimensional matrix facilitated carrier segregation. In the case of modulation-doped $BiCuSeO/Bi_{0.75}Ba_{0.25}CuSeO$ composites [27], the sample is actually a two-phase composite with the modulation doping enabled by carrier delocalization across the grain boundaries (i.e., crystalline disorder) separating the BiCuSeO matrix and the $Bi_{0.75}Ba_{0.25}CuSeO$ inclusions. In fact, all previous modulation-doped materials required interfaces and boundaries in the crystalline lattice (e.g., interfaces in superlattices, anisotropy in layered compounds, and phase boundaries in nanocomposites) to ensure that the free-carrier regions are both spatially and chemically separated from the donor regions or regions with lower carrier concentrations. Modulation doping in a high-quality single crystal with a structurally and chemically homogeneous lattice with only spatially varying *charge* has never been realized, to the best of our knowledge.

Here, we report on the charge and heat transport processes in a class of epitaxial modulation-doped thin films in which the spatial separation of electronic charge densities is achieved without perturbing the parent crystal's compositional or structural homogeneity. Unlike the previous realizations of modulation doping in crystals, our materials demonstrate periodic layering of spatially segregated, varying electronically donor-doped regions in a single compositionally and structurally homogenous single-crystalline lattice; in other words, while these modulation-doped single lattice films contain discrete and sharp *electronic* boundaries, they do not contain any *morphological* or *chemical* boundaries or interfaces in the lattice. Thus, we refer to these modulation-doped nanomaterials as "modulation-doped epitaxial crystals" (MoDECs).

We demonstrate the formation of MoDECs using superlattices composed of alternating layers of yttrium-doped and intrinsic (unintentionally/oxygen vacancy-doped) cadmium oxide (Y:CdO and *i*-CdO, respectively). The small electronic potential that confines electrons within the doped layers, coupled with the epitaxial and crystalline nature of the MoDECs and lack of lattice interfaces, presents a platform to study charge transport and the electron thermal boundary resistances across electronic interfaces. It is well known that structural boundaries in an otherwise crystalline lattice or interfaces between chemically dissimilar crystals can give rise to phonon scattering events and phonon thermal boundary resistances that reduce the thermal conductivity of the composite material [15,30–36]. In our MoDECs, with an order-of-magnitude electronic contrast between each layer, but less than 1% chemical contrast, these phonon-phonon interfacial resistances are nominally absent, offering unimpeded phonon thermal conductivity in these single-crystalline systems. We note that doping CdO leads to an increase in electronic thermal conductivity and a corresponding decrease in the phonon contribution to thermal conductivity [37]. The thermal conductivity of intrinsic CdO is dominated by phonon transport with only a minor contribution from electrons [37]. While increasing the dopant concentration in CdO to improve the electronic-based functionality will reduce the phonon contribution to thermal conductivity, this phononic contribution can still play a non-negligible role in heat conduction, depending on the atomic densities of the dopant atoms [37]. Thus, phonon conduction that is unimpeded by interfaces can offer improved temperature regulation and thermal management in devices based on MoDECs.

However, given the presence of an electronic superlattice with periodically varying carrier concentration and electronic mobility, a question arises: do these electronic interfaces impede electronic and/or thermal transport, and what are the primary heat transport processes that dictate the thermal conductivity of MoDECs? Given that both the *i*-CdO and Y:CdO constituents have fairly high electronic conductivity, the thermal conductivities of *i*-CdO/Y:CdO MoDECs are expected to contain significant electronic contributions [37]. Here, we aim to determine if the electric potential that confines electrons within the Y:CdO layers presents additional electronic or thermal resistances to the overall material. We find not only that *i*-CdO and Y:CdO layers are perfectly electronically coupled but also that modulation doping enhances electronic mobility within one or both constituents by up to 15%. Our analysis further suggests that the thermal boundary resistances across the low potential-energy electronic interfaces are negligible, and the thermal conductivity of MoDECs is controllable based on the electronic thermal conductivities of the doped layers comprising the sample. The thermal conductivities of the MoDEC samples range from ~8 to 12 $W\,m^{-1}\,K^{-1}$, depending on volume fraction of the yttrium-doped cadmium oxide in the MoDECs. These thermal conductivities can be described from a series resistance model of the diffusive thermal resistances of the parent materials comprising the individual layers of the MoDECs, with negligible influence of the thermal boundary resistances at the electronic *i*-CdO/Y:CdO interfaces.

To the best of our knowledge, nanoscale multilayer films made up of parent materials that have notably different transport properties yet composite thermal conductivities that exhibit negligible influences from the thermal boundary resistances at the internal interfaces have never been previously realized [16]. Indeed, even in the case of metal/metal multilayers, where thermal boundary resistances at the metal/metal interfaces are some of the lowest values ever measured for solid/solid interfaces (~0.07–0.25 $m^2\,KGW^{-1}$), the thermal conductivities of the metal/metal composites are substantially reduced compared to the thermal conductivities of the parent materials comprising the multilayers [12–14]. This marks an important thermophysical property of the MoDECs that is enabled by the lack of lattice interfaces yet electronic potential

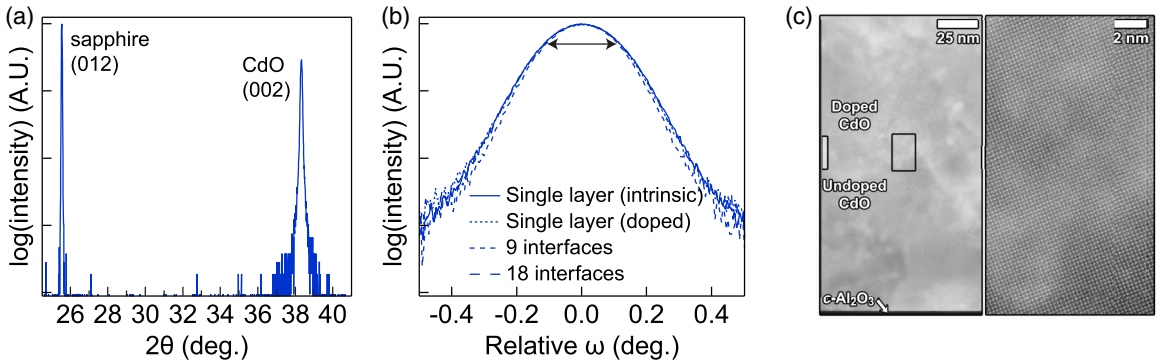

FIG. 1. (a) $2\theta - \omega$ scan of the (002) peak of the CdO MoDEC on sapphire. (b) Rocking curves of the (002) CdO peaks for both single species films and layered MoDECs. There is little to negligible difference in crystallinity between the MoDECs and the CdO films, indicating the MoDECs are single crystalline. (c) ADF STEM of a similar MoDEC sample on c-sapphire, which shows no lattice distortion between layers further confirming the highly crystalline quality of these materials. Doping initiates roughly within the center of the 20-nm long vertical white bar, and the high magnification image (right) taken from the black inset exhibits no lattice distortions across this interface region. Taken together, the XRD and TEM characterizations suggest that the MoDECs are crystallographically indistinguishable from the homogeneous reference films, and the doping and varying modulation periods of the doped layers have negligible impact on the lattice of the films.

barriers that can maintain spatial charge segregation via an interface with negligible impact on thermal transport (i.e., negligible thermal boundary resistances).

We recently demonstrated that doped-CdO thin films exhibit strong, tunable, and low-loss plasmonic absorption in the mid-IR thanks to their exceptionally high electronic mobilities [38,39], offering unique opportunities for mid-IR plasmonic and photonic devices. Modulation-doped CdO systems will further enable unique platforms for mid-IR photonics, such as hyperbolic metamaterials [40,41], optical filters with spatially discrete optical absorption [42,43], or energy harvesting based on charge injection across modulation-doped interfaces [28].

We grew *i*-CdO/Y:CdO superlattices on *r*-plane (012) sapphire at 455 °C via reactive high impulse power magnetron sputtering of a 2-in. pure metallic Cd (99.9999%) target in a mixed Ar/O_2 atmosphere (20/14.4 SCCM, 10 mTorr, where SCCM denotes cubic centimeter per minute at STP). Doping was achieved by applying rf (13.56 MHz) power to a 2-in. metallic yttrium target affixed to a magnetron sputtering source to achieve a target nominal yttrium dopant concentration of $n = 2.1 \times 10^{20}\,\mathrm{cm}^{-3}$ in the CdO. To grow MoDECs, we first deposited a heteroepitaxial *i*-CdO or Y:CdO layer with thickness controlled by deposition rate as calibrated by x-ray reflectivity (XRR). The subsequent alternating doped/intrinsic superlattice layers were grown homoepitaxially, with thickness controlled by calibrated sputtering rates, and doping controlled by a shutter on the yttrium source. Following deposition, the samples were annealed at 700 °C under 1 atm O_2 for 30 min. to maximize oxygen uptake. X-ray-diffraction (XRD) symmetric 2θ-ω scans and rocking curves [Figs. 1(a) and 1(b)] confirm that the MoDECs are indeed epitaxial/crystalline, with crystalline quality directly comparable to *i*-CdO and Y:CdO monolayer reference samples. Annular dark-field scanning transmission electron microscopy (ADF STEM) of a similar modulation-doped sample, grown on *c*-plane (0001) sapphire with In doping, finds no evidence for structural changes induced by dopant layering in sputtered CdO films. In the low magnification ADF STEM image Fig. 1(c), a vertically oriented white bar of length ~20 nm is centered on the position where doping transitions from undoped-to-doped CdO, though this leads to no identifiable changes in image. A higher magnification micrograph acquired in the region marked with the black overlay shows no discernable changes in the atomic-scale structuring of the CdO lattice across the interface. This is consistent with our previous work [44], where we show that the addition of doping in CdO films has minimal effect on both the in- and out-of-plane lattice parameters of CdO. Furthermore, from our XRD data in Fig. 1, we determine a lattice parameter in our samples of 4.694 Å, within 0.05% of the bulk lattice constant of CdO [45], and within our experimental uncertainty. Additionally, the overlapping rocking curves of the various MoDECs and reference CdO films in Fig. 1(b) suggest that the MoDECs are crystallographically indistinguishable from the homogeneous reference films. This suggests that the doping and varying modulation periods of the doped layers have negligible impact on the lattice of the films, and that our samples are strain relaxed.

Here, we study MoDECs with 2, 3, 5, 9, or 18 alternating layers, which corresponds to interface densities of 0.0056, 0.011, 0.022, 0.044, and $0.094\,\mathrm{nm}^{-1}$, respectively. The total thickness of each MoDEC is nominally 180 nm, with the thickness of the constituent layers controlled so that total volume of *i*-CdO and Y:CdO is constant across each MoDEC sample set. We grew three different sample sets, with *i*-CdO to Y:CdO thickness ratios of 1:3, 1:1, and 3:1, hereafter referred to as $(\mathrm{CdO})_{0.25}/(\mathrm{Y:CdO})_{0.75}$, $(\mathrm{CdO})_{0.5}/(\mathrm{Y:CdO})_{0.5}$, and $(\mathrm{CdO})_{0.75}/(\mathrm{Y:CdO})_{0.25}$. Table I contains further description of each MoDEC, including the nominal thickness of each layer. We additionally grew two 180-nm-thick single-layer thin films of *i*-CdO ($n = 1.9 \times 10^{19}\,\mathrm{cm}^{-3}$; $\mu = 355\,\mathrm{cm}^2/\mathrm{V\,s}$) and Y:CdO ($n = 2.1 \times 10^{20}\,\mathrm{cm}^{-3}$; $\mu = 423\,\mathrm{cm}^2/\mathrm{V\,s}$) as reference samples, where n is the carrier density and μ is the mobility. Prior to measuring the thermal conductivity of each sample, we deposited 80 nm of Al on the film surface using electron-beam evaporation. The overall thicknesses of each sample and the Al transducer were measured using XRR.

TABLE I. Nominal thicknesses of each layer in the MoDEC superlattice samples.

	$(CdO)_{0.25}/(Y:CdO)_{0.75}$	$(CdO)_{0.5}/(Y:CdO)_{0.5}$	$(CdO)_{0.75}/(Y:CdO)_{0.25}$
2 layers	Al_2O_3 //135 nm Y:CdO // 45 nm *i*-CdO	Al_2O_3 //90 nm Y:CdO // 90 nm *i*-CdO	Al_2O_3 //45 nm Y:CdO // 135 nm *i*-CdO
3 layers	Al_2O_3 //22.5 nm *i*-CdO // 135 nm Y:CdO // 22.5 nm *i*-CdO	Al_2O_3 //45 nm *i*-CdO // 90 nm Y:CdO //45 nm *i*-CdO	Al_2O_3 //67.5 nm *i*-CdO // 45 nm Y:CdO //67.5 nm *i*-CdO
5 layers	Al_2O_3 //[15 nm *i*-CdO // 67.5 nm Y:CdO] × 2 // 15 nm *i*-CdO	Al_2O_3 //[30 nm *i*-CdO // 45 nm Y:CdO] × 2 // 30 nm *i*-CdO	Al_2O_3 //[45 nm *i*-CdO // 22.5 nm Y:CdO] × 2 // 45 nm *i*-CdO
9 layers	Al_2O_3 //[9 nm *i*-CdO // 33.75 nm Y:CdO] × 4 //9 nm *i*-CdO	Al_2O_3 //[18 nm *i*-CdO // 22.5 nm Y:CdO] × 4 // 18 nm *i*-CdO	Al_2O_3 //[27 nm *i*-CdO // 11.25 nm Y:CdO] × 4 // 27 nm *i*-CdO
18 layers	Al_2O_3 //[15 nm Y:CdO // 5 nm *i*-CdO] × 9	Al_2O_3 //[10 nm Y:CdO // 10 nm *i*-CdO] × 9	Al_2O_3 //[5 nm Y:CdO // 15 nm *i*-CdO] × 9

We quantified the electronic properties of each sample via Hall effect measurements. Figure 2(a) shows that all of the MoDEC samples are conductive, with well-delineated conductivities that are similar to the conductivity of single layers grown with the equivalent average carrier concentration of the MoDEC, i.e., the $(CdO)_{0.25}/(Y:CdO)_{0.75}$ samples have a nominal average $n = 0.25(1.9 \times 10^{19}\,cm^{-3}) + 0.75(2.1 \times 10^{20}\,cm^{-3}) = 1.5 \times 10^{20}\,cm^{-3}$. Notably, the electronic conductivity of each MoDEC is clearly *enhanced* relative to single-layer films, especially in the three- to nine-layer superlattices. Hall effect measurements reveal that this conductivity enhancement arises primarily from an increased overall electronic mobility in multilayer samples, while the carrier concentration follows the law of averages. Based on a multilayer model for Hall effect measurements (see Supplemental Material [46]), this effect is a clear signature of strong electronic coupling between the *i*-CdO and Y:CdO layers, with negligible resistance at the electronic interface [47,48]. Furthermore, our multilayer electronic model shows that the increased mobility measured over the full MoDEC stacks can only be explained by either a simultaneous mobility enhancement of up to 17% across both of the *i*-CdO/Y:CdO constituents or a mobility enhancement of up to 68% within one constituent. Considering that the mobility enhancement is greatest in the $(CdO)_{0.75}/(Y:CdO)_{0.25}$ samples, we speculate that through modulation doping Y:CdO layers donate electrons to the *i*-CdO layers in the vicinity of the electronic interface to neutralize ionized point defects; our model predicts an effective 68% mobility increase within the *i*-CdO layers from 355 to 596 $cm^2/V\,s$ in the most extreme case. While microscopic evidence for this hypothesis is beyond the scope of this Rapid Communication, a similar effect, with a fourfold mobility increase, has already been observed at SnTe/CdO interfaces [47]. Finally, finite-element simulations

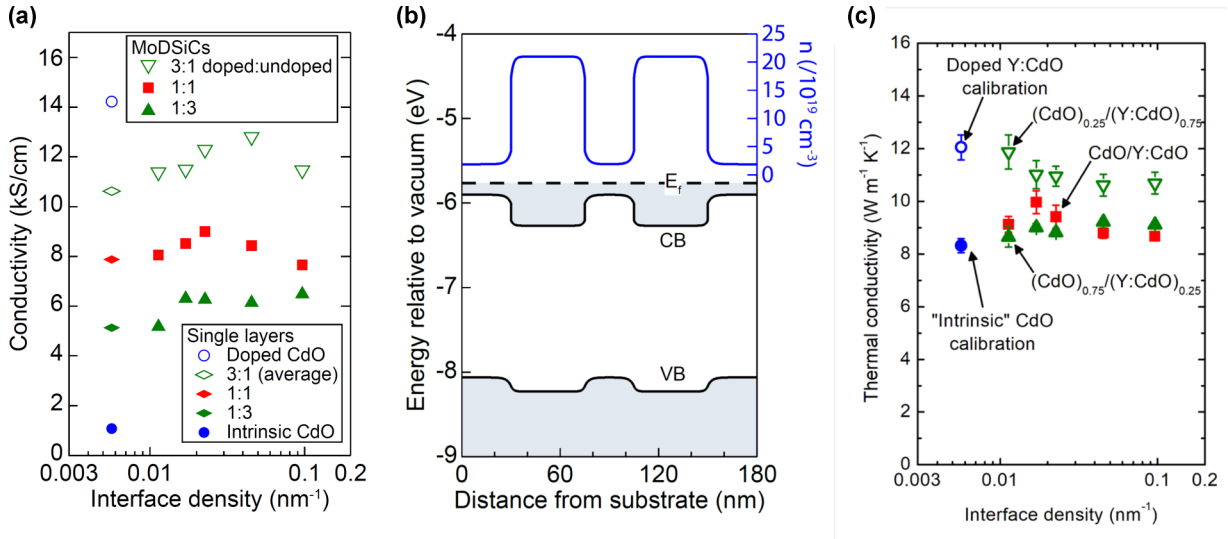

FIG. 2. (a) Conductivity vs interfacial density of MoDECs, as measured by Hall measurements. Conductivity scales with overall concentration of carriers. (b) Finite-element simulations of Poisson's equation for a five-layer CdO MoDEC, showing carriers are well confined to the more highly doped layers. (c) Thermal conductivity of all three MoDEC sample series. The thermal conductivities of all MoDECs lie in-between the thermal conductivities of the single species control films.

[COMSOL Multiphysics, Fig. 2(b)] of Poisson's equation in *i*-CdO/Y:CdO MoDECs confirm that electronic charge is localized within individual layers in our MoDECs films. Because of the large and degenerate electron concentrations throughout the MoDEC thickness, and because the electron concentration of the Y:CdO layers is more than an order of magnitude larger than in the *i*-CdO layers, the depletion/accumulation regions in the superlattices are exceptionally short, on the order of 1–5 nm. Thus, over the thickness of the MoDECs, the carrier concentration is expected to have a strongly localized boxlike profile. The 18-layered MoDECs are an important exception, as the layers become thin enough that the depletion/accumulation lengths are comparable to the layer thickness (see Supplemental Material [46]). Importantly, IR-reflectivity measurements of our MoDECs, along with Drude model-based fits using the transfer-matrix method, allowed us to experimentally confirm charge separation and rule out dopant/carrier intermixing by diffusion (see Supplemental Material [46]).

We measured the thermal conductivities of each MoDEC using time domain thermoreflectance (TDTR) [12,32,49–51]. Details of our TDTR measurements and analysis are found in the Supplemental Material [46]. The thermal conductivities of the CdO-based MoDECs and calibration films are shown in Fig. 2(c). We note that all thermal conductivities reported in this Rapid Communication represent the thermal conductivity in the cross-plane direction, perpendicular to the interfaces.

We measure the cross-plane thermal conductivity of the intrinsic and doped CdO control films as 8.2 and 12.1 $\mathrm{W\,m^{-1}\,K^{-1}}$, respectively. Using the Wiedemann-Franz law applied to our in-plane electrical conductivity measurements [Fig. 2(a)], we then estimate the in-plane electron thermal conductivity of the *i*-CdO and Y:CdO films as 0.8 and 10.4 $\mathrm{W\,m^{-1}\,K^{-1}}$, respectively. Thus, this suggests that the thermal transport in the intrinsic layers is primarily dominated by phonon conduction, where electrons contribute to the majority of thermal conductivity in the doped layers (i.e., $>80\%$ of the total thermal conductivity is from electrons in the doped layers). This is consistent with our previous findings on Dy-doped CdO [37]. Given the cubic symmetry of CdO and ability to separate the influence of film/substrate interfaces from the intrinsic cross-plane thermal conductivity of these CdO films, comparing the in-plane-derived electron thermal conductivity to the TDTR-measured total thermal conductivity is acceptable for estimating the relative electron and phonon contributions to thermal conductivity.

The general trend among all MoDEC samples is that the thermal conductivity changes with increasing interface density relative to the *i*-CdO and Y:CdO controls up to about 0.02 interfaces/nm, at which point the thermal conductivity is relatively constant. However, the way in which the thermal conductivity changes with interface density depends on the relative thicknesses of the doped and undoped layers. For example, increasing interfacial density reduces the thermal conductivity of the $(CdO)_{0.25}/(Y:CdO)_{0.75}$ samples relative to the Y:CdO control. Conversely, the thermal conductivity is higher in the $(CdO)_{0.75}/(Y:CdO)_{0.25}$ and $(CdO)_{0.50}/(Y:CdO)_{0.50}$ samples relative to the intrinsic CdO control. Above an interface density of 0.02 interfaces/nm, the thermal conductivities of the $(CdO)_{0.75}/(Y:CdO)_{0.25}$ and $(CdO)_{0.50}/(Y:CdO)_{0.50}$ are relatively similar and lower than that of the $(CdO)_{0.25}/(Y:CdO)_{0.75}$.

In previous works studying the thermal conductivity of multilayers and superlattices, the thermal conductivities of these systems are always lower than those of the individual materials that comprise the structures. For example, in Cu/Nb and Pt/Ir multilayers, the thermal conductivities are less than those of Cu and Nb, or Pt and Ir, respectively [13,14]. This is due to the electron thermal boundary resistances at the metal/metal interfaces that drive down the total thermal conductivity of the multilayer films [13,52,53]. The same holds true with metal/nonmetal [54–56] and nonmetal/nonmetal [5,16,19,21,57] superlattices, where in these cases the phonon thermal boundary resistances typically play the dominant resistor role. In the case of our MoDECs, we see a different trend: simply increasing the volume fraction of the higher thermal conductivity material that comprises the MoDEC leads to an increase in thermal conductivity. This implies that any potential interfacial resistances in the electronic or phononic subsystems in the MoDECs are negligible (i.e., electron-electron, electron-phonon, phonon-phonon).

To test this hypothesis, we measured the thermal conductivity of a series of films with equivalent carrier densities as the average carrier concentrations in the MoDEC films, as they should have an equivalent contribution from the carriers, without any potential barriers from the electronic interfaces. Figure 3 shows the thermal conductivity of the Y:CdO films as a function of average carrier density in the CdO. In line with our previous experiments, the thermal conductivity of the CdO increases with carrier density due to an increase in the electronic contribution to thermal conductivity [37,38]. Also shown in Fig. 3 are the thermal conductivities of the MoDEC samples from Fig. 2 plotted as a function of average carrier density across the entire sample thickness. We determine the carrier densities of the MoDECs by performing a weighted average of the carrier concentrations of the yttrium-doped and intrinsic regions based on the volume fraction of each layer. The thermal conductivities of these MoDECs are calculated by averaging the thermal conductivity data in Fig. 2 over all samples with an interface density greater than or equal to 0.02 interfaces/nm, where the error bars represent the standard deviation among these data.

The similarities between the MoDEC samples and the single-layer samples with equivalent carrier densities suggest that the electronic interfaces that exist between the Y-doped and intrinsic CdO layers do not pose any appreciable resistance to heat transport. Furthermore, as previously mentioned, since there are no lattice interfaces or changes in crystallinity in the MoDEC samples, a phonon thermal boundary resistance does not exist in these samples. Thus, our experimental data suggest that the thermal conductivities of these MoDECs are driven by parallel phononic and electronic contributions, with the electronic portion dictated by the summation of the electronic contributions in both the intrinsic and yttrium-doped layers.

To support this conclusion, we model the thermal conductivity of the MoDECs using a series thermal resistance

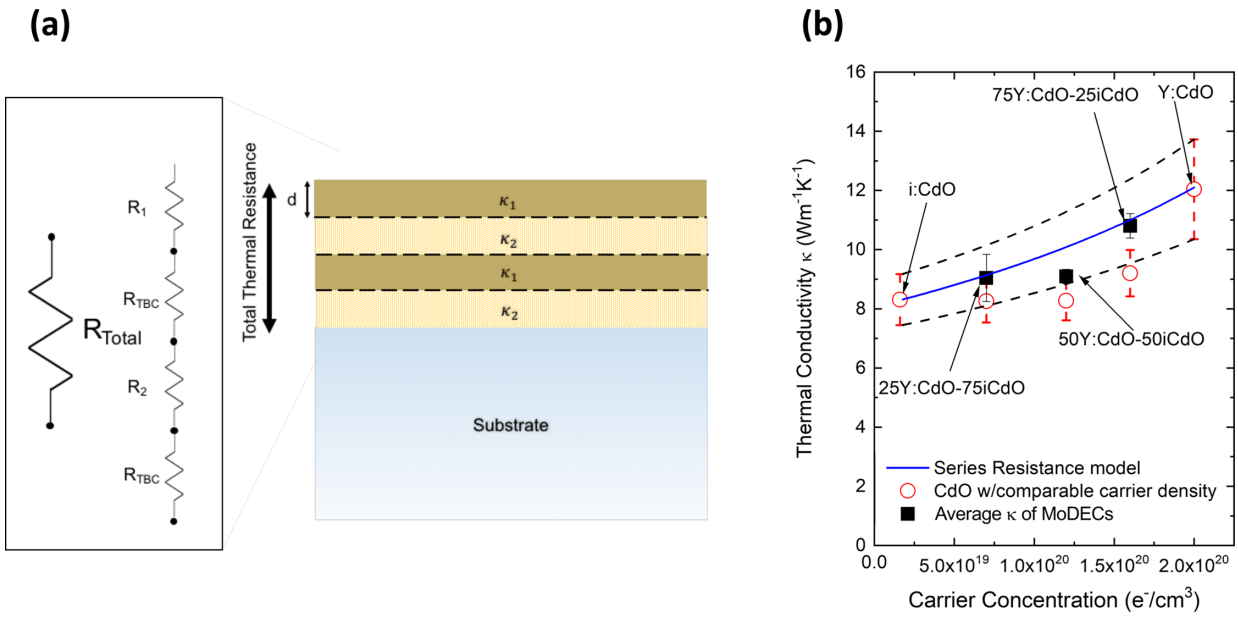

FIG. 3. (a) Thermal resistance model for a MoDEC. The total thermal resistance of a MoDEC sample (R_{total}) is the sum of the resistances of each layer and the thermal boundary resistances at the interfaces. (b) The blue line is the calculated thermal conductivity of a MoDEC with a concentration of Y:CdO going from 0 to 100% calculated via Eq. (2) (where the dotted lines represent the uncertainty of this calculation), assuming $R_{\text{int}} = 0$. The black squares are the average thermal conductivities of the three different MoDEC series. The red circles are the thermal resistance of single species CdO films with a comparable carrier concentration as the corresponding MoDEC. The agreement confirms that the electronic interfaces offer negligible thermal resistance.

approach, where

$$\kappa_{\text{MoDEC}} = \frac{d_{\text{total}}}{R_{\text{total}}} = (R_{\text{Y:CdO}} + R_{i-\text{CdO}} + R_{\text{int}})^{-1} \qquad (1)$$

where d_{total} is the total thickness of the MoDEC and R_{total} is its thermal resistance of the MoDEC sample, $R_{\text{Y:CdO}}$ is the thermal resistance of the yttrium-doped CdO layer, $R_{i-\text{CdO}}$ is the thermal resistance of the intrinsic CdO layer, and R_{int} is the thermal boundary resistance at the Y:CdO/*i*-CdO interface; this model is graphically depicted in Fig. 3(a). From our previous discussion, we assume $R_{\text{int}} = 0$, thus Eq. (1) becomes

$$\kappa_{\text{MoDEC}} = (R_{\text{Y:CdO}} + R_{i-\text{CdO}})^{-1} = \left(\frac{d_{\text{Y:CdO}}}{\kappa_{\text{Y:CdO}}} + \frac{d_{i-\text{CdO}}}{\kappa_{i-\text{CdO}}}\right)^{-1} \qquad (2)$$

where d is the total thickness of the Y:CdO or *i*-CdO layers in the sample. Calculations of Eq. (2) are shown in Fig. 3 (solid blue line), where we assume $\kappa_{\text{Y:CdO}} = 12.0 \pm 1.7\,\text{W m}^{-1}\,\text{K}^{-1}$ and $\kappa_{i-\text{CdO}} = 8.3 \pm 0.9\,\text{W m}^{-1}\,\text{K}^{-1}$ from the calibrations shown in Fig. 2; the dashed lines are the calculations of Eq. (2) when accounting for the uncertainty in $\kappa_{\text{Y:CdO}}$ and $\kappa_{i-\text{CdO}}$. The agreement between our model calculations and experimental data on the MoDEC support our hypothesis that $R_{\text{int}} = 0$. Thus, in our MoDEC, the series contributions to the thermal conductivity of the electrons from each layer behave as isolated resistors, and the sum of all the resistors dictates the overall resistance of the structure, with negligible resistance from the potential barrier at the Y:CdO/*i*-CdO interface. Stated differently, a rule of mixtures adequately describes the overall thermal resistance of the MoDEC, similar to the heat transport processes in more traditionally studied superlattices.

Based on our discussion above, we can estimate a maximum resistance associated with the electronic potential barrier at the Y:CdO/*i*-CdO interface. In the highest interface density samples, the average thicknesses of the Y:CdO and *i*-CdO layers are 10 nm. This corresponds to thermal resistances of each layer of $R_{\text{Y:CdO}} = 10 \times 10^{-9}/\kappa_{\text{Y:CdO}} = 0.8\,\text{m}^2\,\text{K GW}^{-1}$ and $R_{i-\text{CdO}} = 10 \times 10^{-9}/\kappa_{i-\text{CdO}} = 1.2\,\text{m}^2\,\text{K GW}^{-1}$, yielding a MoDEC resistance of $2.0\,\text{m}^2\,\text{K GW}^{-1}$. To yield a non-negligible change in total resistance of the MoDEC, which we assume as a ~18% change based on the uncertainties reported in our calculations of Eq. (2) and shown in Fig. 3(b), the thermal resistances at the Y:CdO/*i*-CdO interfaces must be greater than $R_{\text{int}} > 0.4\,\text{m}^2\,\text{K GW}^{-1}$ (rounding up based on precision). Thus, we estimate that the maximum possible thermal resistance at these Y:CdO/*i*-CdO interfaces is $0.4\,\text{m}^2\,\text{K GW}^{-1}$. Stated differently, the lowest possible electron thermal boundary conductance across the electronic potential barrier formed at the Y:CdO/*i*-CdO interface is $2.5\,\text{GW m}^{-2}\,\text{K}^{-1}$, a relatively high thermal boundary conductance that is typical for interfaces between two regions of different electronic carrier concentration, and consistent with prior works studying the thermal boundary conductance across metal/metal interfaces [12–14].

In summary, we have demonstrated the formation of a class of epitaxial modulation-doped thin films in which the spatial separation of electronic charge densities is achieved without perturbing the parent crystal's compositional or structural homogeneity. Unlike the previous realizations of modulation doping in crystals, our materials demonstrate periodic layering of spatially segregated, varying electronically

donor-doped regions in a single compositionally and structurally homogenous single-crystalline lattice. We form these "modulation-doped epitaxial crystals" using alternating layers of doped/intrinsic cadmium oxide, and from this our Rapid Communication demonstrates the ability to spatially confine regions of variable carrier concentration via low potential-energy barriers in a spatially homogeneous single crystal with a chemically and structurally homogenous lattice (i.e., no chemical or structural lattice interfaces). The low potential energy that confines electrons within the doped layers coupled with the single-crystal nature of the MoDECs and lack of lattice interfaces presents a platform to study the electron thermal boundary resistances at low-energy electronic barriers. We measure the cross-plane thermal conductivity of an array of MoDECs with different electronic interface densities and assess the various heat transport mechanisms, including the role of the electronic interfaces separating the variably doped regions. We find that any potential thermal boundary resistances in the electronic or phononic subsystems in the MoDECs are negligible, the series contributions to thermal conductivity of the electrons from each layer behave as isolated resistors, and the sum of all the resistors dictates the overall thermal resistance of the structure with negligible resistance from the potential barrier at the Y:CdO/*i*-CdO interface. This is in stark contrast with other nanoscale multilayer materials, where thermal boundary resistances at the internal material interfaces reduce the thermal conductivity of the multilayer compared to that of the parent materials. This marks an important thermophysical property of the MoDECs that is enabled by the lack of lattice interfaces yet electronic potential barriers that can maintain spatial charge segregation via an interface with negligible impact on thermal transport (i.e., negligible thermal boundary resistances). Based on the resistances of the individual layers in the MoDECs, we estimated the maximum possible thermal boundary resistance as $0.4\,\mathrm{m^2\,K\,GW^{-1}}$ (or a minimum possible thermal boundary conductance $2.5\,\mathrm{GW\,m^{-2}\,K^{-1}}$), ensuring that the thermal resistance across the electronic potential barrier remains relatively negligible as compared to the thermal resistances of the layers in the MoDECs. This low value of electron-electron thermal boundary resistance is consistent with those measured across metal/metal interfaces. The ability to modulation dope these MoDEC systems and systematically tune their thermal resistances will further enable unique platforms for mid-IR photonics, such as hyperbolic metamaterials, optical filters with spatially discrete optical absorption, or energy harvesting based on charge injection across modulation-doped interfaces.

We acknowledge funding from the Army Research Office, Multidisciplinary University Research Initiative (Grant No. W911NF-16-1-0406). E.D.G. and J.M.L. gratefully acknowledge support from the NSF (Grant No. DMR-1350273). E.D.G. acknowledges support for this work through a NSF Graduate Research Fellowship (Grant No. DGE-1252376). This work was performed in part at the Analytical Instrumentation Facility (AIF) at North Carolina State University, which is supported by the State of North Carolina and the NSF (Grant No. ECCS-1542015). The AIF is a member of the North Carolina Research Triangle Nanotechnology Network, a site in the National Nanotechnology Coordinated Infrastructure.

[1] A. J. Minnich, M. S. Dresselhaus, Z. F. Ren, and G. Chen, Bulk nanostructured thermoelectric materials: Current research and future prospects, Energy Environ. Sci. **2**, 466 (2009).

[2] M. Zebarjadi, K. Esfarjani, M. S. Dresselhaus, Z. F. Ren, and G. Chen, Perspectives on thermoelectrics: From fundamentals to device applications, Energy Environ. Sci. **5**, 5147 (2012).

[3] A. D. Rakic, A. B. Djurisic, J. M. Elazar, and M. L. Majewski, Optical properties of metallic films for vertical-cavity optoelectronic devices, Appl. Opt. **37**, 5271 (1998).

[4] S. Clark, P. Ahirwar, F. Jaeckel, C. Hains, A. Albrecht, P. Schjetnan, T. J. Rotter, L. R. Dawson, G. Balakrishnan, P. E. Hopkins, L. M. Phinney, J. Hader, and J. V. Moloney, Growth and thermal conductivity analysis of polycrystalline GaAs on CVD diamond for use in thermal management of high-power semiconductor lasers, J. Vac. Sci. Technol. B **29**, 03C130 (2011).

[5] R. Cheaito, C. A. Polanco, S. Addamane, J. Zhang, A. W. Ghosh, G. Balakrishnan, and P. E. Hopkins, Interplay between total thickness and period thickness in the phonon thermal conductivity of superlattices from the nanoscale to the microscale: Coherent versus incoherent phonon transport, Phys. Rev. B **97**, 085306 (2018).

[6] G. Chen and C. L. Tien, Facet heating of quantum well lasers, J. Appl. Phys. **74**, 2167 (1993).

[7] Q. Zhou, A. S. Cross, Y. Fu, A. Beling, B. M. Foley, P. Hopkins, and J. C. Campbell, Balanced InP/InGaAs photodiodes with 1.5-W output power, IEEE Photonics J. **5**, 6800307 (2013).

[8] Q. Zhou, A. S. Cross, F. Yang, A. Beling, and J. C. Campbell, Development of narrowband modified uni-travelling-carrier photodiodes with high power efficiency, in Proceedings of the 2013 IEEE Avionics, Fiber-Optics, and Photonics Conference, 2013 (unpublished), pp. 65–66.

[9] M. Ren, S. Maddox, Y. Chen, M. Woodson, J. C. Campbell, and S. Bank, AlInAsSb/GaSb staircase avalanche photodiode, Appl. Phys. Lett. **108**, 081101 (2016).

[10] M. E. Woodson, M. Ren, S. J. Maddox, Y. Chen, S. R. Bank, and J. C. Campbell, Low-noise AlInAsSb avalanche photodiode, Appl. Phys. Lett. **108**, 081102 (2016).

[11] Y. Shen, J. T. Gaskins, X. Xie, B. M. Foley, R. Cheaito, P. E. Hopkins, and J. C. Campbell, Thermal analysis of high-power flip-chip-bonded photodiodes, J. Lightwave Technol. **35**, 4242 (2017).

[12] R. Cheaito, C. S. Gorham, A. Misra, K. Hattar, and P. E. Hopkins, Thermal conductivity measurements via time-domain thermoreflectance for the characterization of radiation induced damage, J. Mater. Res. **30**, 1403 (2015).

[13] R. Cheaito, K. Hattar, J. T. Gaskins, A. K. Yadav, J. C. Duda, T. E. Beechem, J. F. Ihlefeld, E. S. Piekos, J. K. Baldwin,

A. Misra, and P. E. Hopkins, Thermal flux limited electron Kapitza conductance in copper-niobium multilayers, Appl. Phys. Lett. **106**, 093114 (2015).

[14] R. B. Wilson and D. G. Cahill, Experimental Validation of the Interfacial form of the Wiedemann-Franz Law, Phys. Rev. Lett. **108**, 255901 (2012).

[15] D. G. Cahill, W. K. Ford, K. E. Goodson, G. D. Mahan, A. Majumdar, H. J. Maris, R. Merlin, and S. R. Phillpot, Nanoscale thermal transport, J. Appl. Phys. **93**, 793 (2003).

[16] P. M. Norris, N. Q. Le, and C. H. Baker, Tuning phonon transport: From interfaces to nanostructures, J. Heat Transfer **135**, 061604 (2013).

[17] G. Chen, Size and interface effects on thermal conductivity of superlattices and periodic thin-film structures, J. Heat Transfer **119**, 220 (1997).

[18] G. Chen, Thermal conductivity and ballistic-phonon transport in the cross-plane direction of superlattices, Phys. Rev. B **57**, 14958 (1998).

[19] G. Chen, *Nanoscale Energy Transport and Conversion: A Parallel Treatment of Electrons, Molecules, Phonons, and Photons* (Oxford University, New York, 2005).

[20] M. N. Luckyanova, J. Garg, K. Esfarjani, A. Jandl, M. T. Bulsara, A. J. Schmidt, A. J. Minnich, S. Chen, M. S. Dresselhaus, Z. Ren, E. A. Fitzgerald, and G. Chen, Coherent phonon heat conduction in superlattices, Science **338**, 936 (2012).

[21] J. Ravichandran, A. K. Yadav, R. Cheaito, P. B. Rossen, A. Soukiassian, S. J. Suresha, J. C. Duda, B. M. Foley, C.-H. Lee, Y. Zhu, A. W. Lichtenberger, J. E. Moore, D. A. Muller, D. G. Schlom, P. E. Hopkins, A. Majumdar, R. Ramesh, and M. A. Zurbuchen, Crossover from incoherent to coherent phonon scattering in epitaxial oxide superlattices, Nat. Mater. **13**, 168 (2014).

[22] S. Y. Ren and J. D. Dow, Thermal conductivity of superlattices, Phys. Rev. B **25**, 3750 (1982).

[23] R. Dingle, H. L. Störmer, A. C. Gossard, and W. Wiegmann, Electron mobilities in modulation-doped semiconductor heterojunction superlattices, Appl. Phys. Lett. **33**, 665 (1978).

[24] H. L. Störmer, R. Dingle, A. C. Gossard, W. Wiegmann, and M. D. Sturge, Two-dimensional electron gas at a semiconductor-semiconductor interface, Solid State Commun. **88**, 933 (1993).

[25] A. Samarelli, L. F. Llin, S. Cecchi, J. Frigerio, T. Etzelstorfer, E. Müller, Y. Zhang, J. R. Watling, D. Chrastina, G. Isella, J. Stangl, J. P. Hague, J. M. R. Weaver, P. Dobson, and D. J. Paul, The thermoelectric properties of Ge/SiGe modulation doped superlattices, J. Appl. Phys. **113**, 233704 (2013).

[26] S. R. Wood, D. R. Merrill, G. Mitchson, A. C. Lygo, S. R. Bauers, D. M. Hamann, D. R. Sutherland, J. Ditto, and D. C. Johnson, Modulation doping in metastable heterostructures via kinetically controlled substitution, Chem. Mater. **29**, 773 (2017).

[27] Y.-L. Pei, H. Wu, D. Wu, F. Zheng, and J. He, High thermoelectric performance realized in a BiCuSeO system by improving carrier mobility through 3D modulation doping, J. Am. Chem. Soc. **136**, 13902 (2014).

[28] B. Yu, M. Zebarjadi, H. Wang, K. Lukas, H. Wang, D. Wang, C. Opeil, M. Dresselhaus, G. Chen, and Z. Ren, Enhancement of thermoelectric properties by modulation-doping in silicon germanium alloy nanocomposites, Nano Lett. **12**, 2077 (2012).

[29] M. Zebarjadi, G. Joshi, G. Zhu, B. Yu, A. Minnich, Y. Lan, X. Wang, M. Dresselhaus, Z. Ren, and G. Chen, Power factor enhancement by modulation doping in bulk nanocomposites, Nano Lett. **11**, 2225 (2011).

[30] P. L. Kapitza, The study of heat transfer in helium II, Zh. Eksp. Teor. Fiz. **11**, 1 (1941).

[31] E. T. Swartz and R. O. Pohl, Thermal boundary resistance, Rev. Mod. Phys. **61**, 605 (1989).

[32] P. E. Hopkins, Thermal transport across solid interfaces with nanoscale imperfections: Effects of roughness, disorder, dislocations, and bonding on thermal boundary conductance, ISRN Mech. Eng. **2013**, 682586 (2013).

[33] B. F. Donovan, B. M. Foley, J. F. Ihlefeld, J.-P. Maria, and P. E. Hopkins, Spectral phonon scattering effects on the thermal conductivity of nano-grained barium titanate, Appl. Phys. Lett. **105**, 082907 (2014).

[34] L. Chen, J. L. Braun, B. F. Donovan, P. E. Hopkins, and S. J. Poon, Ballistic transport of long wavelength phonons and thermal conductivity accumulation in nanograined silicon-germanium alloys, Appl. Phys. Lett. **111**, 131902 (2017).

[35] B. M. Foley, H. J. Brown-Shaklee, J. C. Duda, R. Cheaito, B. J. Gibbons, D. Medlin, J. F. Ihlefeld, and P. E. Hopkins, Thermal conductivity of nano-grained $SrTiO_3$ thin films, Appl. Phys. Lett. **101**, 231908 (2012).

[36] A. D. McConnell and K. E. Goodson, Thermal conduction in silicon micro- and nanostructures, Annu. Rev. Heat Transfer **14**, 129 (2005).

[37] B. F. Donovan, E. Sachet, J.-P. Maria, and P. E. Hopkins, Interplay between mass-impurity and vacancy phonon scattering effects on the thermal conductivity of doped cadmium oxide, Appl. Phys. Lett. **108**, 021901 (2016).

[38] E. Sachet, C. T. Shelton, J. S. Harris, B. E. Gaddy, D. L. Irving, S. Curtarolo, B. F. Donovan, P. E. Hopkins, P. A. Sharma, A. L. Sharma, J. F. Ihlefeld, S. Franzen, and J. P. Maria, Dysprosium-doped cadmium oxide as a gateway material for mid-infrared plasmonics, Nat. Mater. **14**, 414 (2015).

[39] E. L. Runnerstrom, K. P. Kelley, E. Sachet, C. T. Shelton, and J.-P. Maria, Epsilon-near-zero modes and surface plasmon resonance in fluorine-doped cadmium oxide thin films, ACS Photonics **4**, 1885 (2017).

[40] A. Poddubny, I. Iorsh, P. Belov, and Y. Kivshar, Hyperbolic metamaterials, Nat. Photonics **7**, 948 (2013).

[41] A. J. Hoffman, L. Alekseyev, S. S. Howard, K. J. Franz, D. Wasserman, V. A. Podolskiy, E. E. Narimanov, D. L. Sivco, and C. Gmachl, Negative refraction in semiconductor metamaterials, Nat. Mater. **6**, 946 (2007).

[42] Z. Sun, A. Martinez, and F. Wang, Optical modulators with 2D layered materials, Nat. Photonics **10**, 227 (2016).

[43] A. Mazuelas, R. Hey, B. Jenichen, and H. T. Grahn, Alternating Be and C doping for strain compensated GaAs/AlAs distributed Bragg reflectors, Appl. Phys. Lett. **70**, 2088 (1997).

[44] K. P. Kelley, E. Sachet, C. T. Shelton, and J.-P. Maria, High mobility yttrium doped cadmium oxide thin films, APL Materials **5**, 076105 (2017).

[45] D. Strauch, CdO: Lattice parameters, in *New Data and Updates for Several III-V (Including Mixed Crystals) and II-VI Compounds*, edited by U. Rössler (Springer, New York, 2012), pp. 77–79.

[46] See Supplemental Material at http://link.aps.org/supplemental/10.1103/PhysRevMaterials.3.032201 for details of time

domain thermoreflectance measurements, dislocation density effects on CdO thermal conductivity and thermal boundary conductances, validation of series resistor analysis of thermal transport on the MoDECs, spatial segregation of free carriers in the MoDECs, Hall effect measurements, and midinfrared reflectivity measurements.

[47] J. Nishitani, K. M. Yu, and W. Walukiewicz, Charge transfer and mobility enhancement at CdO/SnTe heterointerfaces, Appl. Phys. Lett. **105**, 132103 (2014).

[48] B. Arnaudov, T. Paskova, S. Evtimova, E. Valcheva, M. Heuken, and B. Monemar, Multilayer model for Hall effect data analysis of semiconductor structures with step-changed conductivity, Phys. Rev. B **67**, 045314 (2003).

[49] D. G. Cahill, Analysis of heat flow in layered structures for time-domain thermoreflectance, Rev. Sci. Instrum. **75**, 5119 (2004).

[50] A. J. Schmidt, Pump-probe thermoreflectance, Annu. Rev. Heat Transfer **16**, 159 (2013).

[51] P. E. Hopkins, J. R. Serrano, L. M. Phinney, S. P. Kearney, T. W. Grasser, and C. T. Harris, Criteria for cross-plane dominated thermal transport in multilayer thin film systems during modulated laser heating, J. Heat Transfer **132**, 081302 (2010).

[52] B. C. Gundrum, D. G. Cahill, and R. S. Averback, Thermal conductance of metal-metal interfaces, Phys. Rev. B **72**, 245426 (2005).

[53] P. E. Hopkins, T. E. Beechem, J. C. Duda, J. L. Smoyer, and P. M. Norris, Effects of subconduction band excitations on thermal conductance at metal-metal interfaces, Appl. Phys. Lett. **96**, 011907 (2010).

[54] V. Rawat, Y. K. Koh, D. G. Cahill, and T. D. Sands, Thermal conductivity of (Zr,W)N/ScN metal/semiconductor multilayers and superlattices, J. Appl. Phys. **105**, 024909 (2009).

[55] P. Jha, T. D. Sands, L. Cassels, P. Jackson, T. Favaloro, B. Kirk, J. Zide, X. Xu, and A. Shakouri, Cross-plane electronic and thermal transport properties of p-type $La_{0.67}Sr_{0.33}MnO_3$/$LaMnO_3$ perovskite oxide metal/semiconductor superlattices, J. Appl. Phys. **112**, 063714 (2012).

[56] B. Saha, Y. R. Koh, J. Comparan, S. Sadasivam, J. L. Schroeder, M. Garbrecht, A. Mohammed, J. Birch, T. Fisher, A. Shakouri, and T. D. Sands, Cross-plane thermal conductivity of (Ti,W)N/(Al,Sc)N metal/semiconductor superlattices, Phys. Rev. B **93**, 045311 (2016).

[57] Y. K. Koh, Y. Cao, D. G. Cahill, and D. Jena, Heat-transport mechanisms in superlattices, Adv. Funct. Mater. **19**, 610 (2009).